

# PHOTON STRUCTURE \*

GÜNTER GRINDHAMMER

Max-Planck-Institut für Physik, (Werner-Heisenberg-Institut), D-80805 München, Germany  
E-mail: guenterg@desy.de

Large  $p_T$  processes at HERA, initiated by almost real and by virtual photons, provide information on the structure of the photon. We report on the latest measurements of dijets and large  $p_T$  particle production with the H1 detector. This includes a leading order determination of an effective virtual photon parton density, of the gluon density of the photon, and comparisons with models.

## 1 What is a photon?

A photon is not just a photon and not just a hadron. In the leading order (LO) QCD framework it has two components, a direct one, which couples electromagnetically to the partons in the proton for example, and a resolved one. In its resolved state it fluctuates either into an on-shell  $q\bar{q}$ -pair forming a vector meson (VDM part) or an off-shell  $q\bar{q}$ -pair (anomalous part), including any number of gluons, which may interact strongly with other partons around. In pictorial form this is expressed in Fig. 1. In dijet or large  $p_T$  particle production in  $ep$  collisions

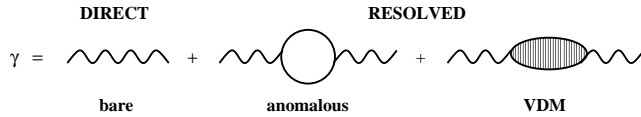


Figure 1: The dual nature of the photon and its associated nomenclature.

we have two important scales to consider, the virtuality of the photon  $Q^2$  and the mean  $\bar{E}_t$  of the hard jets or the large  $p_T$  of an outgoing charged particle. In order to gain some intuition about the effect of the two scales, it is instructive to compare the life-times of the  $e\gamma$ -state and the  $q\bar{q}$ -fluctuation of the photon. Making use of the Heisenberg uncertainty relation, we find that the life-time of the  $e\gamma$ -state falls like  $1/Q^2$  (i.e. from  $O(10000)$  fm to  $O(100)$  fm for  $Q^2$  from 0.1 to 100  $\text{GeV}^2$ ). The life-time of the  $q\bar{q}$ -fluctuation is constant for fixed  $p_T$  such that the photon lives long enough do develop into a  $q\bar{q}$  or even more complicated state as long as  $Q^2 < p_T^2$ . In this situation, in  $ep$  collisions, the partons in the proton are able to probe the partons in the photon target. However with increasing  $Q^2$ , i.e. decreasing life-time of the photon, the photon becomes less resolvable.

The hadronic structure of the photon has been well established both through measurements of the real photon structure in  $\gamma\gamma$  collisions at  $e^+e^-$  colliders (PETRA, PEP, and LEP) and the measurements of jets in photoproduction at HERA. Extending these measurements to the virtual photon structure is expected to provide new insight into the QCD framework, linking deep-inelastic

(DIS),  $\gamma p$ , and  $\gamma\gamma$  interactions.

## 2 What is being measured at HERA?

In LO QCD we expect contributions to dijet production from the direct processes of photon-gluon fusion and QCD-Compton and the resolved  $2 \rightarrow 2$  parton processes shown in Fig. 2. In next-to-leading order (NLO) direct

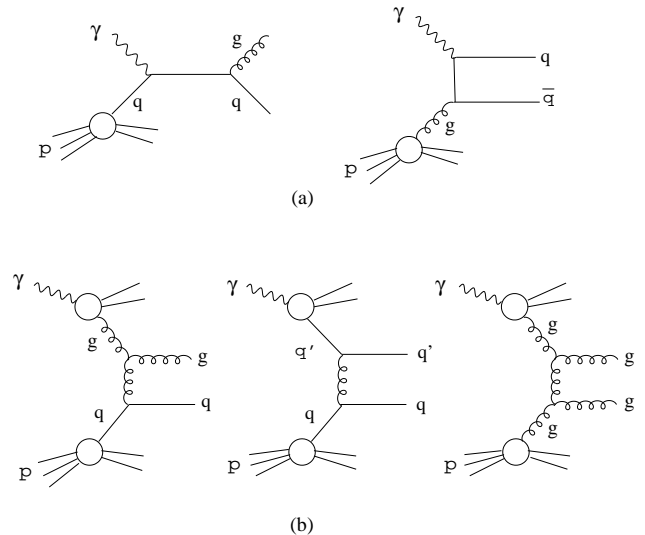


Figure 2: LO direct (a) and resolved processes (b)

and resolved processes can no longer be distinguished. Experimentally, the hard scale  $Q^2$  and the fractional energy of the photon,  $y$ , are determined from the measurement of the energy and angle of the scattered electron. The variable  $x_\gamma^{\text{jets}}$ , correlated with the fractional energy,  $x_\gamma$ , of the parton in the photon participating in the hard scattering process is determined from the energy and direction of the two hardest jets and all of the hadrons in the event, using:

$$x_\gamma^{\text{jets}} = \frac{\sum_{jet1}^{jet2} (E_{jet} - p_{z,jet})}{\sum_h (E_h - p_{z,h})}. \quad (1)$$

\*Talk given on behalf of the H1 Collab., ICHEP'98, Vancouver, Canada, July 22-30, 1998.

By cutting on  $x_\gamma^{\text{jets}}$ , enriched event samples due to either direct or resolved processes can be obtained. At the parton level  $x_\gamma^{\text{jets}} = 1$  for direct processes.

The resolved  $ep$  cross section can be written as:

$$\sigma_{\text{res}}^{ep} \sim \frac{f_{\gamma/e}(y, Q^2)}{y} \sum_{i,j}^{N_f} \frac{f_{i/\gamma}(x_\gamma, E_T^2, Q^2)}{x_\gamma} \frac{f_{j/p}(x_p, E_T^2)}{x_p} |M_{ij}|^2, \quad (2)$$

where the sum runs over all  $2 \rightarrow 2$  hard scattering matrix elements, folded by the density of parton  $j$  in the proton and parton  $i$  in the photon, and finally folded by the density of the photon in the electron. In the fractional energy,  $x_p$ , of the parton in the proton, the measurement covers the range from about 0.01 to 0.1, where the parton densities of the proton are well known.

The H1 experiment has selected events in the range  $1.6 < Q^2 < 80 \text{ GeV}^2$  and  $0.1 < y < 0.7$  in their most recent dijet analysis<sup>1,2</sup>. The jet selection was performed in the  $\gamma^*p$  center of mass system (cms) using the inclusive  $k_t$  algorithm<sup>3</sup>. Events were required to have at least two jets satisfying the following criteria:

$$|\eta_{\text{jet1}} - \eta_{\text{jet2}}| < 1.0, \quad -3.0 < \bar{\eta} < -0.5, \\ \bar{E}_t^2 > 30 \text{ GeV}^2, \text{ and } \frac{E_{T,\text{jet1}} - E_{T,\text{jet2}}}{E_{T,\text{jet1}} + E_{T,\text{jet2}}} < 0.25, \quad (3)$$

where  $\bar{\eta}$  and  $\bar{E}_t$  are the mean pseudorapidity ( $\eta = -\ln \tan(\theta/2)$ ) and mean transverse energy of the two highest  $E_T$  jets. The first two cuts make sure that the jets are confined to the acceptance of the detector, where they are well measured and that  $x_\gamma$  is well determined. The restriction on the difference in  $\eta$  of the jets reduces the probability of misidentifying a part of the photon or proton remnant as one of the high  $E_T$  jets. The constraints are such that the highest (second highest)  $E_T$  jet has  $E_T \gtrsim 7$  (4) GeV. This asymmetric jet selection will allow a comparison of the data with NLO calculations. With this selection H1 obtains a sample of  $\sim 12000$  dijet events for an integrated luminosity of  $6 \text{ pb}^{-1}$ .

The dijet cross sections measured as a function of  $x_\gamma$ ,  $\bar{E}_t^2$ , and  $Q^2$  have been corrected for detector acceptance and resolution effects in separate ranges of  $Q^2$  by applying an iterative Bayesian unfolding technique<sup>4</sup> in  $x_\gamma$  and  $\bar{E}_t^2$ . The jet profiles and the pedestal energy outside of the jets are reasonably well described<sup>1,2</sup> by the HERWIG<sup>5</sup> Monte Carlo (MC) used for the unfolding and also by the RAPGAP<sup>6</sup> MC used to estimate uncertainties due to different models. A good description of the pedestal energy, also referred to as soft underlying event<sup>1,2</sup> and in part caused by soft interactions of the photon and proton remnant, is of importance due to the steeply falling  $p_T$  distribution of the jets.

For the virtual photon parton densities the Herwig MC uses the model by Drees and Godbole (DG)<sup>7</sup> for suppressing the parton densities of real photons with increasing  $Q^2$  by interpolating smoothly between the  $\ln(p_T^2/\Lambda_{QCD}^2)$  behavior of real photons and the asymptotic  $\ln(p_T^2/Q^2)$  dependence of the anomalous piece, i.e.:

$$f_{q/\gamma}(x_\gamma, p_T^2, Q^2) = f_{q/\gamma}(x_\gamma, p_T^2, 0) L(p_T^2, Q^2, \omega) \\ f_{g/\gamma}(x_\gamma, p_T^2, Q^2) = f_{g/\gamma}(x_\gamma, p_T^2, 0) L^2(p_T^2, Q^2, \omega), \text{ where} \\ L(p_T^2, Q^2, \omega) = \frac{\ln \{(p_T^2 + \omega^2)/(Q^2 + \omega^2)\}}{\ln \{(p_T^2 + \omega^2)/\omega^2\}}, \quad (4)$$

where  $\omega^2$  is a free parameter to be chosen to describe the data. Another model of virtual photon parton densities is provided by Schuler and Sjöstrand<sup>8</sup>, consisting of a vector meson dominance and a perturbative anomalous component with appropriate  $Q^2$  evolution.

### 3 Triple differential cross section

The corrected triple differential cross section is shown as a function of  $x_\gamma^{\text{jets}}$ ,  $\bar{E}_t^2$ , and  $Q^2$  respectively in<sup>1,2</sup>. In each case the distributions are shown for ranges of the other two variables. Here, due to lack of space, we only show the  $x_\gamma^{\text{jets}}$  distributions in Fig. 3. They can be seen to

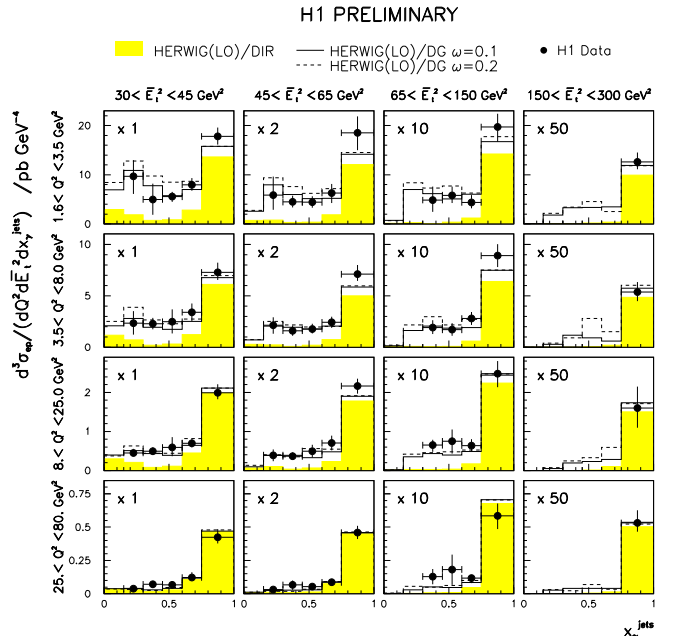


Figure 3: The differential dijet cross section shown as a function of  $x_\gamma^{\text{jets}}$  for different regions of  $\bar{E}_t^2$  and  $Q^2$ . Scale factors applied to the cross section are indicated. The error bars of the data points show the statistical and systematic errors added in quadrature. Also shown are model predictions (HERWIG) with 10% soft underlying event and two choices of the  $Q^2$  suppression factor  $\omega$ . The direct processes as given by this model are indicated as shaded histogram.

peak towards  $x_\gamma^{\text{jets}} = 1$ , where the direct contribution is expected to dominate. For a fixed  $Q^2$  or life-time of the target photon the cross section shows a strong decrease with increasing  $\bar{E}_t^2$  of the probing jet. Increasing  $Q^2$ , i.e. decreasing the life-time of the photon, while keeping the jet  $\bar{E}_t^2$  constant, leads to a decrease of the cross section and a diminishing relative contribution from resolved photons (for  $x_\gamma^{\text{jets}} \leq 0.75$ ). The HERWIG MC using GRV-LO<sup>9</sup> for the parton densities of the real photon and the DG model with  $\omega \sim 0.1$  to 0.2 describes the data. In Fig. 4 the  $Q^2$  dependence of the target photon is shown for a low ( $30 < \bar{E}_t^2 < 45 \text{ GeV}^2$ ) and a high ( $65 < \bar{E}_t^2 < 150 \text{ GeV}^2$ ) range in  $\bar{E}_t^2$  of the probing jet for a bin in  $x_\gamma^{\text{jets}}$  dominated by resolved ( $0.3 < x_\gamma^{\text{jets}} < 0.45$ ) and by direct ( $0.75 < x_\gamma^{\text{jets}} < 1.0$ ) processes. We ob-

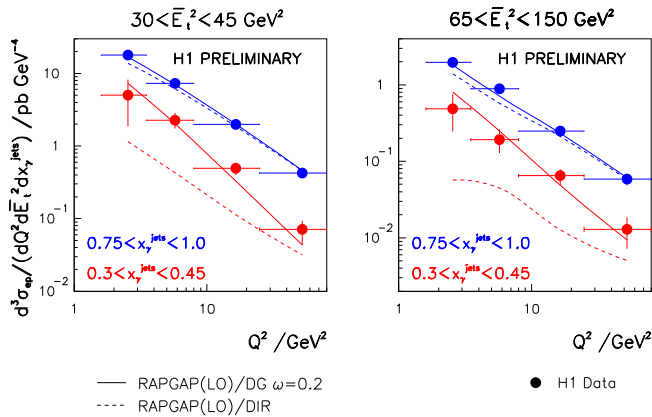


Figure 4: The differential dijet cross section shown as a function of  $Q^2$  for a low and a high range in jet  $\bar{E}_t^2$  and for ranges in  $x_\gamma^{\text{jets}}$  dominated by either direct or resolved processes. Also shown are model predictions (RAPGAP) with a  $Q^2$  suppression factor  $\omega = 0.2$ . The sum of the LO direct and resolved contributions is indicated by the full line, the direct one by the dashed line.

serve a strong decrease of the cross section with  $Q^2$ . The resolved dominated contribution shows an even faster decrease than the direct dominated one. This is what we qualitatively anticipate from the simple considerations in Sect. 1. They are supported quantitatively by the RAPGAP MC as shown in Fig. 4, which is in good agreement with the data. The stronger  $Q^2$  suppression of the resolved contribution is due to the additional  $Q^2$  suppression by the virtual photon parton densities.

We conclude that the observed dependence of the dijet cross section for  $x_\gamma^{\text{jets}} < 0.75$  is consistent with that predicted for a resolved virtual photon with parton densities evolving with  $Q^2$  according to QCD motivated models.

#### 4 Effective virtual photon parton density

In order to determine the parton densities of the virtual photon, H1 has adapted the single effective subprocess (SES) approximation, originally developed for use in  $\bar{p}p$  collisions<sup>10</sup> and recently used to investigate real photon structure<sup>11</sup>. This approximation exploits the fact that the dominant contributions to the cross section comes from  $2 \rightarrow 2$  scattering matrix elements which have similar kinematic dependencies and differ mainly by their associated color factors. Therefore they can be replaced by an effective matrix element,  $M^{\text{SES}}$ , and effective parton densities for the virtual photon,  $\tilde{f}_\gamma$ , and proton,  $\tilde{f}_p$ . The resolved  $ep$  cross section of Eq. 2 then becomes

$$\sigma_{\text{res}}^{\text{SES}} \sim \frac{f_{\gamma/e}(y, Q^2)}{y} \frac{\tilde{f}_\gamma(x_\gamma, p_T^2, Q^2)}{x_\gamma} \frac{\tilde{f}_p(x_p, p_T^2)}{x_p} |M^{\text{SES}}|^2, \quad (5)$$

where the effective parton densities are given by:

$$\tilde{f}_{\gamma,p} = \sum_{N_f} (f_{q/\gamma,p} + f_{\bar{q}/\gamma,p}) + \frac{9}{4} f_{g/\gamma,p} \quad (6)$$

and the sum runs over all quark flavors.

For the extraction of the effective parton density only data with  $0.2 < x_\gamma^{\text{jets}} < 0.7$  and  $E_{T,\text{jet}}^2 > Q^2$ , i.e. the condition for resolving the partons in the photon, are used for a second unfolding to correct the dijet cross section to the LO diparton cross section. This unfolding tries to correct for hadronisation effects and initial and final state QCD radiation. The systematic error<sup>1,2</sup> includes those associated with the determination of the triple differential cross section and additional errors arising in the second unfolding and amounts to an average error of  $\sim 40\%$ .

The resulting effective parton densities, divided by the fine-structure constant  $\alpha$ , are shown in<sup>1,2</sup> as a function of  $x_\gamma$ ,  $p_T^2$ , and  $Q^2$  respectively. In  $x_\gamma$  they show a small rise towards high  $x_\gamma$ , in  $p_T^2$  they are consistent with a scaling behaviour  $\sim \ln p_T^2$ , and in  $Q^2$  they are suppressed with increasing virtuality of the photon as predicted by QCD. They are reasonably well described by GRV-LO and the Drees and Godbole model with  $\omega \sim 0.1$  and the parametrisations SAS-1D and SAS-2D of the model by Schuler and Sjöstrand. In Fig. 5 we show only the results as a function of  $Q^2$  for a fixed scale  $p_T^2 = 85 \text{ GeV}^2$  of the probing jet and two different bins in  $x_\gamma$ . Also shown are two photoproduction data points from H1<sup>11</sup>. The  $Q^2$  evolution of the data are compared to the two models mentioned above and to a single  $\rho$ -pole suppression factor,  $(m_\rho^2/(m_\rho^2 + Q^2))^2$ , characteristic of a simple VMD model. The  $\rho$ -pole factor clearly underestimates the data, while the logarithmic suppression, as expected from QCD with decreasing life-time of the photon, is in agreement with the observation.

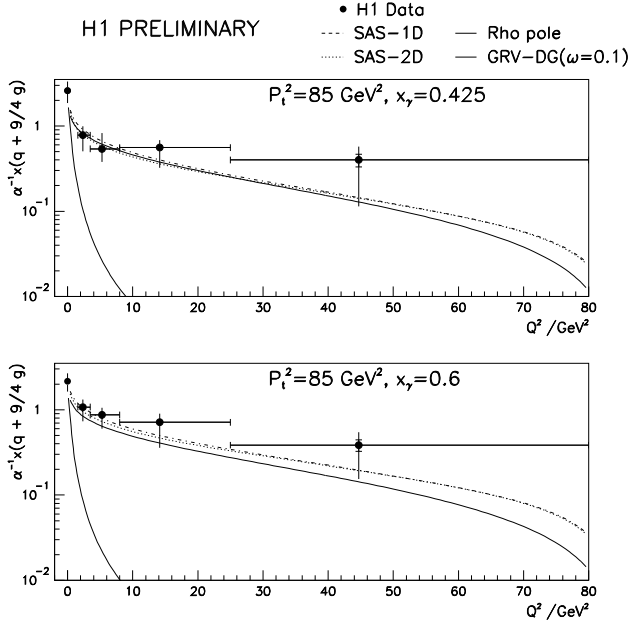


Figure 5: The LO effective parton density of the photon, divided by the fine-structure constant  $\alpha$ , as a function of photon virtuality  $Q^2$  for  $p_T^2 = 85 \text{ GeV}^2$  and two values for  $x_\gamma$ . The error bars of the data points indicate the statistical and systematic errors added in quadrature. Also shown are predictions from the DG model with  $\omega = 0.1$ , using GRV-LO parton densities for real photons and the SAS-1D (dashed line) and SAS-2D (dot-dashed line) parametrisations. The steeply falling solid curve shows the photoproduction data point extrapolated by a  $\rho$ -pole factor.

## 5 Gluon density of the photon

Measurements of the photon structure in  $e^+e^-$  interactions are sensitive to the quark structure of the photon and only indirectly through the QCD evolution to the gluon structure. The data so far have not been precise enough to allow a determination of the gluon density of the photon. Recently, studies of photo-produced dijets and high  $p_T$  charged particles at HERA have shown that these data are sensitive to both the quark and gluon content of the photon. A first measurement by H1 of the LO gluon density<sup>12</sup> showed that it is not large at high  $x_\gamma$ , in contrast to the LAC3<sup>13</sup> parametrisation, and does not have a steep rise towards low  $x_\gamma$  as predicted by the LAC1<sup>13</sup> parametrisation. The minimum  $x_\gamma^{\text{jets}}$  value which was reached in this measurement was 0.04. It is of interest to reach  $x_\gamma$  values as low as possible, since most suggested gluon densities are predicted to rise. Experimentally it is rather difficult to reach low  $x_\gamma$ . Because of the relation  $x_\gamma \sim E_T \exp^{-\eta} / (2E_\gamma)$  for  $Q^2 \sim 0 \text{ GeV}^2$ , low  $x_\gamma$  implies small  $E_T$  (in conflict with a good correlation with the hard dipartons), large  $\eta$  (soft underlying event and detector acceptance), and large  $E_\gamma$  (decreasing event rate).

H1 has contributed two different analyses, one on dijets<sup>14</sup> which is still in progress and one on high  $p_T$  particles<sup>15</sup> which has become final<sup>16</sup> after the conference. The latter analysis does not suffer from the energy scale uncertainty of the calorimeter and is less sensitive to the soft multiple interactions compared to the dijet analysis, but has the drawback of stronger sensitivity to uncertainties in the fragmentation.

Both analyses require the scattered electron to be tagged, which restricts the photon virtuality to  $Q^2 < 0.01 \text{ GeV}^2$ . The energy fraction  $y$  of the radiated photon is required to be in the range 0.5 (0.3 for the high  $p_T$  analysis)  $< y < 0.7$ . In the dijet analysis at least two jets have to be found using a cone algorithm<sup>17</sup> with a cone radius of 0.7. Additional requirements on the jets are:  $p_{T,\text{jets}} > 4 \text{ GeV}$ ,  $M_{\text{jets}} > 12 \text{ GeV}$ ,  $-0.5 < \eta_{\text{jets}} < 2.5$  and  $|\eta_{\text{jets}1} - \eta_{\text{jets}2}| < 1$  in the HERA system. Comparisons of data and MC can be found in<sup>14</sup>. The corrected dijet cross section as a function of  $x_\gamma^{\text{jets}}$ , after unfolding<sup>4</sup>, is shown in Fig. 6. It is compared to LO predictions by the

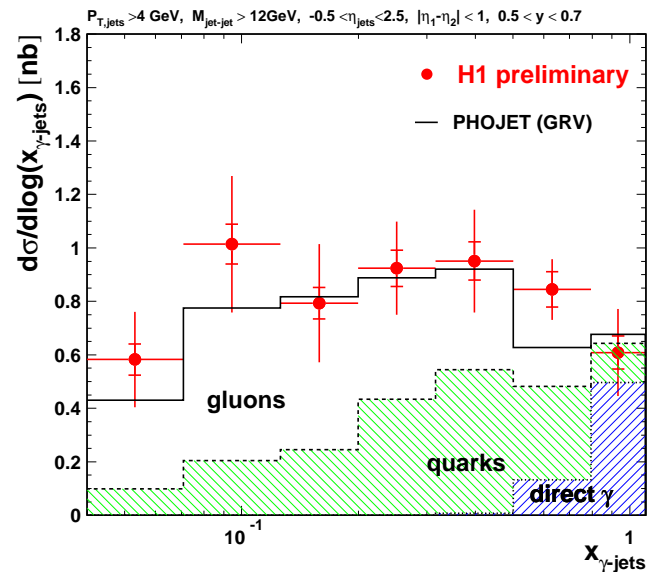


Figure 6: The  $ep$  dijet cross section for  $Q^2 < 0.01 \text{ GeV}^2$  as a function of  $x_\gamma^{\text{jets}}$ . The total error bars on the data points reflect the statistical and systematic errors added in quadrature. The data are compared to a LO model (PHOJET) using the GRV-LO parton densities for the photon and the proton. The contributions from direct and resolved, quark or gluon initiated, processes are indicated.

PHOJET<sup>18</sup> MC using the GRV-LO parton densities for the photon and the proton. The transverse energy  $E_T$  of the jets is used for both the renormalisation and factorisation scale. Also indicated are the different contributions from the direct and resolved processes; the latter are split into contributions initiated from either a quark or a gluon on the photon side. It is clear from the fig-

ure that there is a sizeable contribution from gluons and that the data are precise enough to constrain the gluon density with a precision of  $\approx 30\%$ .

In the high  $p_T$  charged particle analysis the further requirements are: tracks which have a  $p_T > 2$  GeV and  $|\eta| < 1$  in the HERA laboratory frame. In Fig. 7a the corrected  $p_T$  distribution and fits to the H1 and  $\bar{p}p$  data are shown. A QCD inspired power-law expression of the

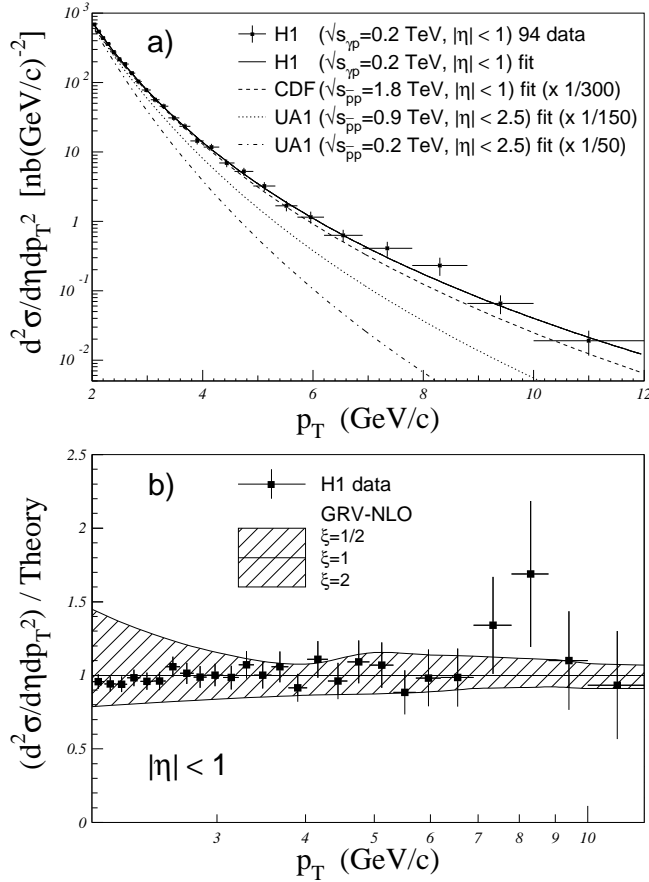


Figure 7: a) The inclusive  $\gamma p$  cross section for charged particles as a function of  $p_T$ . The error bars on the data points denote the statistical and systematic errors added in quadrature. The curves indicate power-law fits to the H1, CDF, and UA1 data; the latter have been normalised to the H1 data at  $p_T = 2$  GeV. b) The ratio of data to an NLO QCD calculation with scale  $\xi p_T^2$ .

form  $A(1 + p_T/p_{T0})^{-n}$  was fit. The fit gives  $A = 5.44 \pm 0.66$  mb and  $n = 7.03 \pm 0.21$  (stat.+syst.) and describes the data well over the whole range in  $p_T$ . Similar fits to  $\bar{p}p$  data from UA1<sup>19</sup> and CDF<sup>20</sup> have been normalised to the  $\gamma p$  cross section at  $p_T = 2$  GeV. The high  $p_T$  tail in the  $\gamma p$  data is clearly larger than in  $\bar{p}p$  collisions at similar cms energies. This can be understood as being due to extra contributions in  $\gamma p$ , namely the direct and the point-like resolved component. Similar conclusions have been obtained for  $\gamma\gamma$  collisions by OPAL<sup>21</sup>.

The ratio of data to theory, as given by an NLO calculation including direct and resolved contributions<sup>22</sup>, and using as scales  $\mu_\gamma^2 = \mu_p^2 = \mu_{\text{had}}^2 = \xi p_{T,\text{had}}^2$  with  $\xi = 1/2, 1$ , and  $2$ , is shown in Fig. 7b. The pseudorapidity distributions for data and the NLO calculation for  $p_T > 2$  and  $p_T > 3$  GeV are given in Fig. 8. The data are well described by NLO, in particular for  $\xi$  close to 1. However, one finds that the NLO prediction is rather sensitive to the choice of scale ( $\xi$ ). This effect is smaller for larger  $p_T$ . For each event with at least one charged particle with

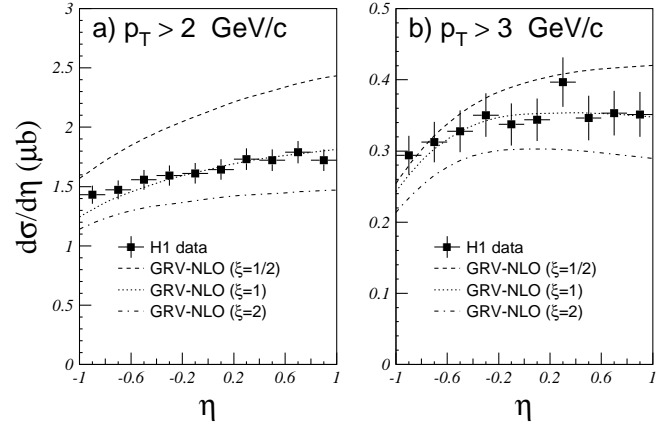


Figure 8: The inclusive  $\gamma p$  cross section as a function of  $\eta$  for charged particles with a)  $p_T > 2$  GeV and b)  $p_T > 3$  GeV in comparison with an NLO QCD calculation with scale  $\xi p_T^2$ . The error bars indicate the statistical and systematic errors added in quadrature.

$p_T > 2.6$  GeV, the variable  $x_\gamma^{\text{rec}} = \sum p_T \exp(-\eta) / E_\gamma$ , where the sum runs over all tracks with  $p_T > 2$  GeV, is calculated. It shows a good correlation<sup>16</sup> to the true  $x_\gamma$ . To obtain  $x_\gamma$  an unfolding procedure<sup>23</sup> was used. Then the LO gluon density was unfolded allowing for an uncertainty in the quark densities of  $\sim 15\%$  as given by three different parametrisations<sup>9,8,13</sup> and using different hadronisation models. The resulting gluon density (only available after the conference) is shown in Fig. 9 as a function of  $x_\gamma$  and compared to an older extraction using dijets<sup>12</sup> and to three different parametrisations. The mean  $p_T^2$  of the hard scattering process for this data sample is  $38 \text{ GeV}^2$  according to MC, which was used as the scale for the comparison with three parton density parametrisations, GRV-LO<sup>9</sup>, SAS-1D-LO<sup>8</sup>, and LAC1-LO<sup>13</sup>. The mean  $p_T^2$  for the dijet sample is  $75 \text{ GeV}^2$ . The results confirm that the contribution of the gluon to the photon structure is significant. The gluon density rises with decreasing  $x_\gamma$  and is best described by GRV-LO.

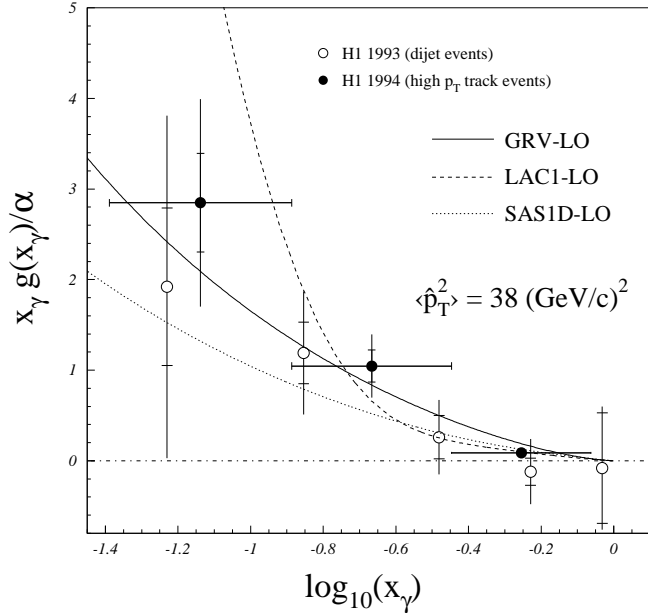


Figure 9: The LO gluon density in the photon from charged high  $p_T$  tracks (full circles) and from dijets (open circles) with a mean scale  $p_T^2 = 38 \text{ GeV}^2$  and  $p_T^2 = 75 \text{ GeV}^2$  respectively. The full error bars give the statistical and systematic errors added in quadrature. The lines show the predictions of three different parametrisations.

## 6 Summary

At HERA, with dijet and high  $p_T$  particle production, we can probe the virtual photon structure over a large range in the scale  $\sim p_T^2$  and in the life-time of the photon  $\sim 1/Q^2$ .

In the measured dijet cross section as well as the extracted effective virtual photon parton density, we observe the expected logarithmic suppression with  $Q^2$ , as the life-time of the photon decreases, of the resolved photon contribution.

Using two complementary methods, high  $p_T$  charged particles and dijets in almost real photoproduction, the leading order gluon density of the photon was determined and found to be rising with decreasing  $x_\gamma$ .

So far we have only scratched the surface in that we have found consistency with rather global expectations and in that we have learned how to do leading order determinations of parton densities. There is a lot more to do, stay tuned for 1999.

## Acknowledgements

I want to thank my colleagues in H1, who helped in preparing the presentation, and Martin Erdmann and Steve Maxfield for reading this manuscript.

## References

1. H1 Coll., paper 544 submitted to this conference.
2. H1 Coll., C. Adloff et al., to be submitted.
3. S. D. Ellis and D. E. Soper, *Phys. Rev. D* **48**, 3160 (1993); S. Catani et al., *Nucl. Phys. B* **406**, 187 (1993).
4. G. D'Agostini, *Nucl. Instrum. Methods A* **362**, 487 (1995).
5. G. Marchesini et al., *Comp. Phys. Comm.* **67**, 465 (1992).
6. H. Jung, *Comp. Phys. Comm.* **86**, 147 (1995).
7. M. Drees and R. Godbole, *Phys. Rev. D* **50**, 3124 (1994); F. M. Borzumati and G. A. Schuler, *Z. Phys. C* **58**, 139 (1993).
8. T. Sjöstrand and G. A. Schuler, *Phys. Lett. B* **376**, 193 (1996).
9. M. Glück, E. Reya, and A. Vogt, *Phys. Rev. D* **46**, 1973 (1992).
10. B. V. Combridge and C. J. Maxwell, *Nucl. Phys. B* **239**, 429 (1984).
11. H1 Coll., C. Adloff et al., *Eur. Phys. J. C* **1**, 97 (1998).
12. H1 Coll., T. Ahmed et al., *Nucl. Phys. B* **445**, 195 (1995).
13. H. Abramowicz, K. Charchula, and A. Levy, *Phys. Lett. B* **269**, 458 (1991).
14. H1 Coll., paper 549 submitted to this conference.
15. H1 Coll., paper 551 submitted to this conference.
16. H1 Coll., C. Adloff et al., DESY 98-148, hep-ex/9810020, submitted to *Eur. Phys. J. C*.
17. J. Huth et al., Proc. Summer Study on HEP, Snowmass, Colorado, (1994) 134; CDF Coll., F. Abe et al., *Phys. Rev. D* **45**, 1448 (1992); L. A. del Pozo, Ph.D. thesis, University of Cambridge, RALT-002, (1993).
18. R. Engel, *Z. Phys. C* **66**, 203 (1995); R. Engel and J. Ranft, *Phys. Rev. D* **54**, 4244 (1996).
19. UA1 Coll., C. Albajar et al., *Nucl. Phys. B* **335**, 261 (1990).
20. CDF Coll., F. Abe et al., *Phys. Rev. Lett.* **77**, 438 (1996).
21. S. Söldner-Rembold, these proceedings.
22. F. M. Borzumati, B. A. Kniel, and G. Kramer, *Z. Phys. C* **59**, 341 (1993); B. A. Kniel and G. Kramer, *Z. Phys. C* **62**, 53 (1994); B. A. Kniel, Proc. Ringberg Workshop, Ringberg Castle, (1997) and hep-ph/9709261.
23. V. Blobel, Proc. CERN School of Computing, Aiguablava, CERN, (1985).